# Observation of structural, mechanical, thermal and microwave dielectric properties of carbon black reinforced PA6/HDPE nanocomposites

Yue Wang[1,2], Zhipeng Niu[1], Haorui Han[1], Jie Wang[1], and Di Lan[1,2,*]

[1] *School of Materials Science and Engineering, Hubei University of Automotive Technology, Shiyan 442002, China*
[2] *Hubei Key Laboratory of Energy Storage and Power Battery, School of Materials Science and Engineering, Hubei University of Automotive Technology, Shiyan 442002, People's Republic of China*

## ABSTRACT

Nylon 6 (PA6) has been widely used in the field of specialty engineering plastics due to its excellent mechanical properties and thermal stability. However, the high water absorption rate of pure PA6 limits its suitability for more complex and demanding environments. In this study, PA6/high-density polyethylene (HDPE)/carbon black (CB) composites were prepared to investigate the effects of different CB contents on the mechanical properties, thermodynamic properties, and transparency of the PA6/PE composites. The results showed that when the CB content reached 4.5%, the composite material exhibited improved tensile strength and impact strength, reaching 53.3 MPa and 13.2 J/m$^2$, respectively. The uniform dispersion of CB within the matrix contributed to more even stress distribution in the composite material and absorbed part of the impact force, and both melting peaks shift towards the left to some extent. Furthermore, the overall real part of the dielectric constant is about 2.5, and dielectric loss tangent of the material reached an extremely low level below 0.01 under this filling ratio. The island-like structure of HDPE and the dispersed CB particles embedded in it exhibited isotropic crystal symmetry. This structure is similar to an isotropic antenna and may play an important role in the transmission of electromagnetic waves. The enhanced comprehensive properties make this PA6-based composite material highly promising in the field of wideband transmission materials.

## 1 Introduction

Microwaves play a crucial role in the transmission of EM information. In devices such as mobile phones, antennas, and antenna covers, materials that allow maximum penetration of EM waves are highly sought after. Polyamide plastics, such as PA6, are widely used and have the largest production volume among engineering plastics. PA6 is known for its excellent mechanical properties, chemical resistance, and high thermal stability [1]. These characteristics make PA6

widely applied in engineering fields such as semiconductors and aerospace industries [2–4].

However, pure PA6 is prone to water absorption and degradation in humid environments, which limits its application in complex environments due to the potential stability issues. On the other hand, HDPE is a common general-purpose plastic known for its good processability, chemical resistance, and electrical insulation properties. Additionally, HDPE has a low moisture absorption rate and does not deform when exposed to moisture [5]. Considering these characteristics, many research groups have explored the blending of PA6 and HDPE to improve the overall properties of the materials.

For instance, Yordanov et al. investigated the blending of low-density polyethylene (LDPE) with PA6 to enhance the material's resistance to hydrolysis and improve its thermal stability by taking advantage of LDPE's low moisture absorption rate. They also studied the blending of PA6 with linear low-density polyethylene (LLDPE) and found that an increase in LLDPE content led to a reduction in moisture absorption and improved impact strength [6]. These studies highlight the potential of blending PA6 with PE to enhance the overall performance of the materials.

Due to the non-polar nature of PE, blending it with PA6 often leads to phase incompatibility, resulting in increased interfacial tension and a decrease in the mechanical properties of the blend system [7]. Overcoming the poor compatibility in blend systems is crucial to maintaining the mechanical properties of the original polymer materials. Malchev et al. [8] addressed this issue by incorporating dispersed glass fibers and matrix glass fibers as reinforcement materials, forming a PE/PA6/GF ternary composite. The results showed that when using dispersed glass fiber reinforcement, the glass fibers were welded together to form a polymer load-bearing matrix, and a continuous fiber network of PA6 was formed on the surface of the glass fibers. This significantly increased the tensile modulus of the composite material and improved its fracture toughness to some extent.

In addition, Kelnar et al. [9] enhanced PE/PA6 composites using organic clay montmorillonite. The montmorillonite can effectively influence the viscosity ratio and interfacial tension between the materials. When a small amount of montmorillonite (2–3%) was added, the blend system exhibited simultaneous improvements in strength, stiffness, and toughness. Liang et al. [10] prepared PA6/carbon fiber (CF) composites through melt extrusion. The results showed that CF was well dispersed in the PA6 matrix, and the strong interfacial adhesion between the matrix and fibers significantly increased the tensile modulus and strength of the materials, by approximately 60 and 50%, respectively. Furthermore, the thermal stability of the PA6/CF composites was also improved.

CB, as a commonly used inorganic filler, is often employed to improve the compatibility between the components of composite materials and enhance their mechanical and dielectric properties [11]. The high specific surface area and porous structure of CB can effectively enhance the mechanical strength of materials [12–15]. Its excellent thermal conductivity allows for efficient conduction of infrared radiation and provides resistance to the effects of ultraviolet radiation, thereby preventing material degradation and aging [16–18]. Additionally, CB exhibits excellent electrical conductivity and adjustable dielectric properties, making it a popular choice for modifying the conductivity and dielectric capabilities of materials [19–21].

In this study, HDPE was first used to toughen and reinforce PA6, and the tensile and thermal properties of PA6/HDPE composites with different gradient ratios were investigated to determine the optimal ratio of the binary polymer blend. Then, different amounts of CB were added to the precursor, and comprehensive control of the mechanical, thermal, and transparency properties of the ternary composite material was achieved. The goal was to obtain a ternary composite material that exhibits excellent performance in the aforementioned aspects. Such a high-performance transparent material has significant potential applications in areas such as radar domes.

## 2 Experimental section

### 2.1 Materials

The High density polyethylene (HDPE, 5000 S) used in this study was purchased from Petrochina Lanzhou Petrochemical Co., Ltd. Nylon 6 (PA6, TP4208) was purchased from Jisheng Industrial Co., Ltd, and Carbon black (CB, AR-3) was purchased from Jisheng Industrial Co., Ltd. The CB were purchased without surface treatment and average particle size is about 30 nm. All chemicals were of analytical grade and could be used directly without further purification.

## 2.2 Preparation of PA6/HDPE/CB

PA6 was dried in a vacuum high-temperature drying oven at 80 °C for 24 h. The three materials, PA6, HDPE, and CB, were then melt-blended in a co-rotating twin-screw extruder. The ratios of PA6/HDPE/CB used were 90/10/1.5, 90/10/3, and 90/10/4.5. The twin-screw extruder had a diameter of 30.8 mm and a length-to-diameter ratio (L/D) of 40. The screw speed was set at 200 rpm/min. The processing temperatures from the feed zone to the die were set at 130 °C, 220 °C, 235 °C, 245 °C, 245 °C, 245 °C, and 250 °C, respectively. The pre-mixed pellets obtained were then fed into a plastic injection molding machine. Using an injection rate of 35 $cm^3$/s at a temperature of 245 ℃, PA6/HDPE/CB specimens were obtained. The four groups of samples were labeled as PHC-0, PHC-1.5, PHC-3, and PHC-4.5, respectively.

## 2.3 Characterization

Attenuated total reflection Fourier-transform infrared (ATR-FTIR, AVATAR360) were used to characterize the types and valence states of elements. The microstructure of the samples was characterized using a high-resolution field emission scanning electron microscope (FESEM, JEOLJSM-7001 F). Differential scanning calorimetry (DSC, Q200DSC) was used to test the thermodynamic properties of the four sample materials.

Tensile Strength Testing: The tensile properties of the samples will be tested using a universal material testing machine at a crosshead speed of 50 mm/min. The tests will be conducted at a temperature of 25 °C. Each group of samples will be tested at least 6 times, and the average values will be analyzed. Impact Strength Testing: standard impact specimens (60 × 10 × 4 mm) will be prepared from the different ratios of PA6/PE/CB composite materials. Six to eight specimens from each group will be tested using an impact testing machine at a pendulum velocity of 3.5 m/s. The data from each group will be recorded. The EM parameters measurements for X-band (8.2–12.4 GHz) were performed using WR-90 coaxial-type rectangular waveguide fixture (Anritsu MS46322B vector network analyzer, BJ100 Coaxial Waveguide Adapter). The WR-90 (8.2 to 12.4 GHz) test fixture required samples with inner dimensions of 22.86 mm (W) × 10.16 mm (H), and all samples were carefully cut to standard sizes to avoid undesired leakage of EM waves.

## 3 Results and discussion

Figure 1 shows the infrared characteristic peaks of the four sample groups. From Fig. 1, it can be observed that with an increasing CB content, the peaks at 2912 and 2843 $cm^{-1}$ correspond to the asymmetric and symmetric stretching vibrations of C–H bonds in CB [22]. The absorption peak between 1500 and 1750 $cm^{-1}$ represents the vibrational absorption peak of specific groups on the surface of CB. The most significant change is observed at 1050 $cm^{-1}$, which corresponds to the stretching vibration peak of double bonds in CB. As the CB content increases, the intensity of this peak gradually increases, indicating a consistent trend with the variation in CB content.

SEM analysis allows us to examine the microstructure and morphology of the materials in detail in Fig. 2. From the 500× electron microscope scanning image, it can be observed that there are many larger spherical particles in the sample, which exhibit a typical "island" structure. The black regions in the background correspond to the PA6 matrix, while the larger irregular white blocks represent HDPE. The distribution of CB in the matrix is indicated by red circles in Fig. 2. Due to the incompatibility between PA6 and HDPE, clear phase interfaces are formed [11]. Zooming in to 1500× magnification, the island structure becomes more prominent. In addition to the PHC-0 composition, small white particles, which are the added carbon black filler, can be observed in all compositions. As the proportion of carbon black increases, the distribution of white particles becomes more uniform. Under the
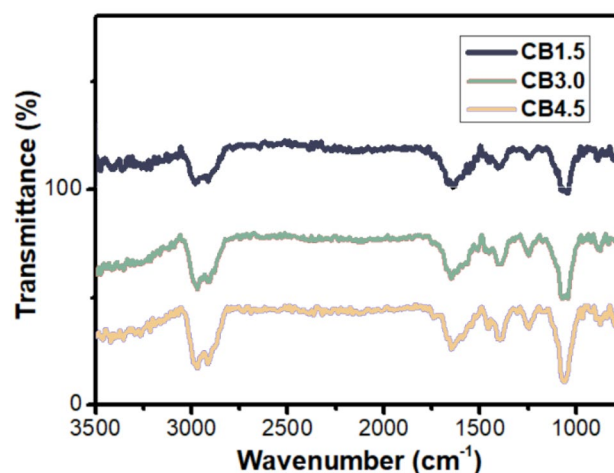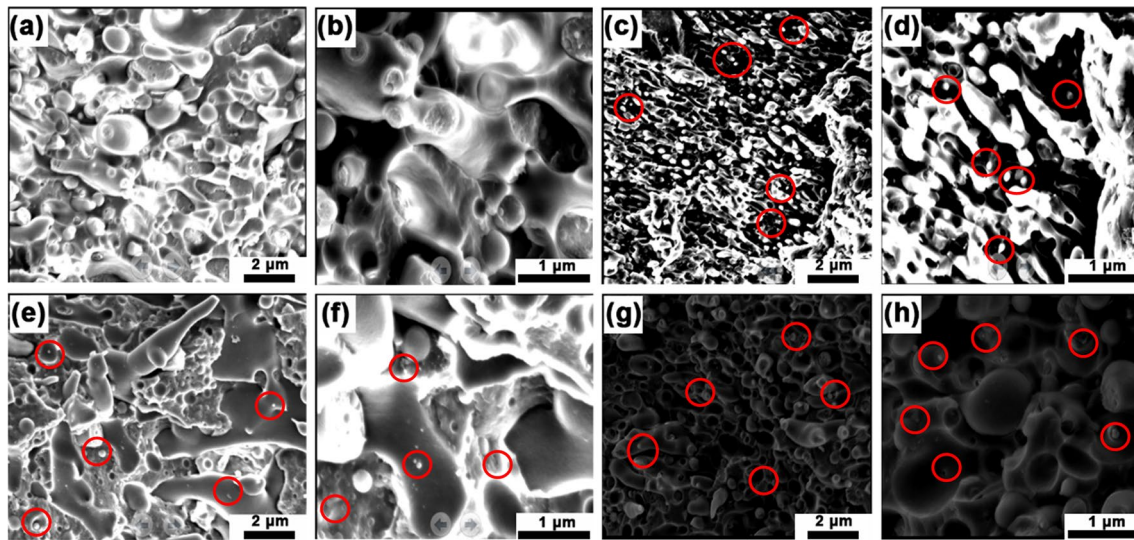


**Fig. 1** FTIR curves of four groups of blend samples

**Fig. 2** SEM image of **a**, **b** PHC-0, **c**, **d** PHC-1.5, **e**, **f** PHC-3 and **g**, **h** PHC-4.5, the magnification of a, c, e and g is 400, and that of b, d, f and h is 1000

1500× magnification, some spherical recessed holes can be observed. These holes are formed when the island structure on this section is pulled out and adheres to another interface during sample fracture, resulting in the island-like structure with these holes. Notably, in the 1.5 and 4.5% carbon black samples at 1500× magnification, many carbon black particles are wrapped in PE. This is due to the shearing force, which causes the accumulation of carbon black particles at the edges and hinders the arrangement of HDPE, resulting in the inclusion of carbon black particles within HDPE. Macroscopically, this leads to an increase in impact strength. As the carbon black content increases, this phenomenon becomes more pronounced.

In the EDS spectrum analysis, the cross-sections of the samples with different carbon black contents were characterized using point analysis, focusing on the elements C, N, and O. From Fig. 3, we can observe that the spectrum shows the presence of elements C, N, O, Al, and Au. This can be attributed to the sandpaper polishing and gold spraying treatment performed on the samples prior to testing. The spectrum reveals that the element with the highest content is C, followed by O. This is because both PA6 and PE, the constituents of the material, contain these two elements. The N element originates from PA6, and since the filler in the sample is carbon black, the majority of the elements are C, as also evident from the elemental distribution map. From the distribution maps of C, N, and O, it can be seen that the C element is uniformly distributed in the materials with different carbon black contents. The N and O elements exhibit a trend of initially increasing and then decreasing with increasing carbon black content. The best effect is observed at a carbon black content of 3%, which further confirms the results obtained from the electron microscope analysis: PA6 as the continuous phase and PE as the dispersed phase, contributing to the enhancement of mechanical properties [23–25].

The melting heat of each component was obtained by testing the three cycle cyclic DSC curves of the four groups of samples, and the calculation was carried out. The crystallinity was obtained through the formula as shown in Table 1; Fig. 4.

From Table 1, it can be observed that the crystallinity of the PHC composite materials, which contain added carbon black as filler, is higher compared to the unfilled PHC-0 composition. This indicates that the addition of carbon black serves as heterogeneous nucleating agent for both PA6 and HDPE, providing multiple nucleation sites and promoting the crystallization of the two phases. As a result, the molecular chains are more orderly arranged in the lattice, leading to higher crystallinity in the polymer blend. In Fig. 4, it is evident that PA6 and PE, being thermodynamically incompatible, exhibit two distinct melting peaks on the thermogram. With the incorporation of carbon black, both melting peaks shift towards the left to
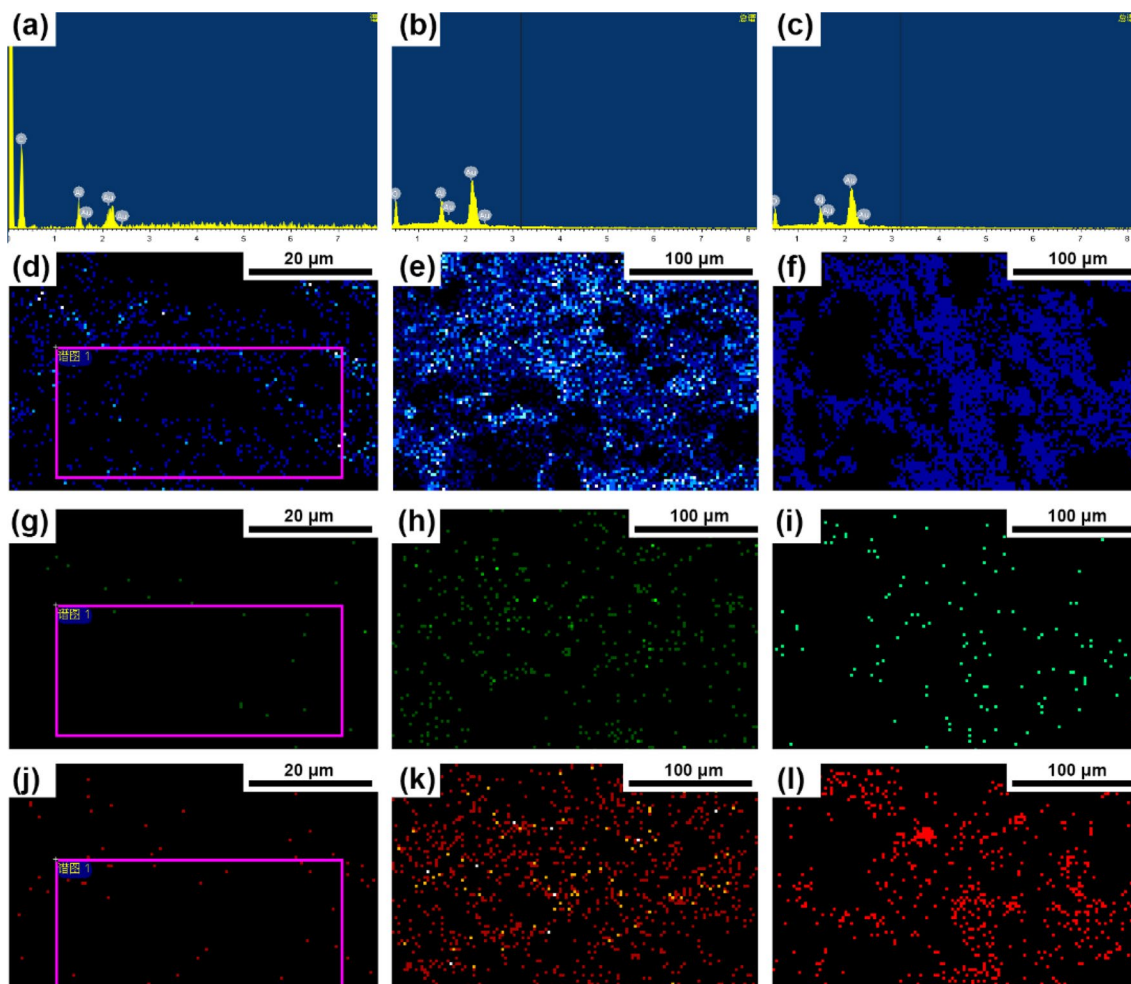
**Fig. 3** SEM-EDS of **a**, **d**, **g**, **j** PHC-1.5, **b**, **e**, **h**, **k** PHC-3 and **c**, **f**, **i**, **l** PHC-4.5

**Table 1** Thermodynamic properties (DSC) data of four groups of samples

| Samples | PA6 | | PE | |
|---|---|---|---|---|
| | Tm/°C | Xc/% | Tm/°C | Xc/% |
| PHC-0 | 220.07 | 16.62 | 132.04 | 6.05 |
| PHC-1.5 | 223.01 | 23.7 | 134.84 | 15.23 |
| PHC-3 | 223.00 | 20.62 | 134.89 | 15.12 |
| PHC-4.5 | 222.75 | 19.74 | 135.18 | 14.59 |

some extent, indicating an improvement in the thermodynamic properties of the PA6/HDPE blend.

In order to show the mechanical properties of the four groups of samples more directly, the relevant stress–strain curves and tensile strength comparisons are shown in Fig. 5. Based on the stress–strain curve, it is evident that the tensile
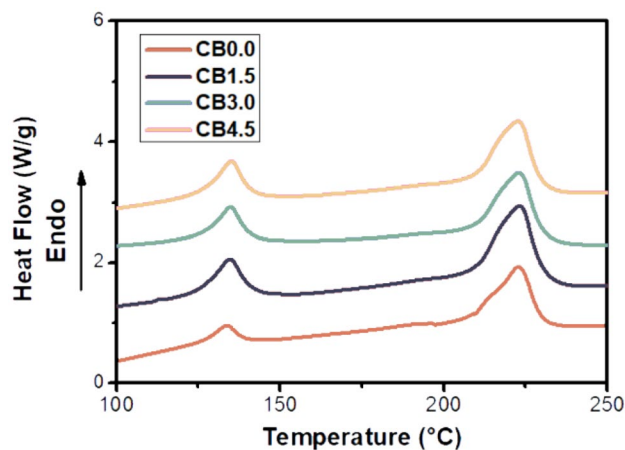


**Fig. 4** DSC thermodynamic curves of PA6/HDPE blends with different CB content
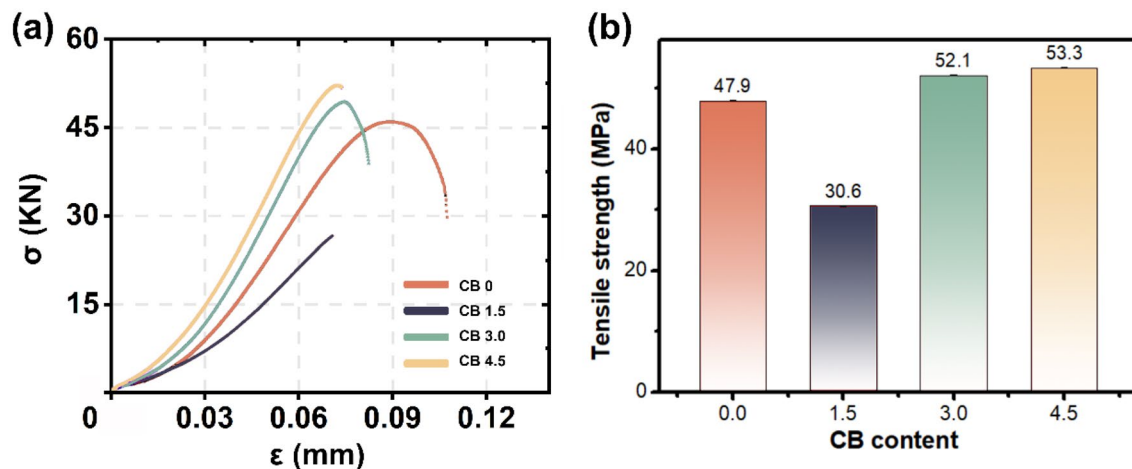
**Fig. 5** Stress–strain curves and tensile strength histogram of four samples, four colors correspond to four sets of samples

strength of the composite materials follows the order: PHC-4.5 > PHC-3 > PHC-0 > PHC-1.5. Carbon black (CB) is commonly used as a reinforcing agent in industry, and hence the addition of 4.5 and 3% CB significantly improves the mechanical properties compared to the unfilled 90% PA6/10% PE base composite. The trend of the tensile properties of PA6/HDPE/CB composite materials shows a first decrease and then an increase with increasing CB content, as shown in Fig. 5. When the CB content is 1.5%, the mechanical properties of the composite material decrease compared to the unfilled PA6/PE composite. This decrease is attributed to the uneven distribution of CB within the polymer matrix, leading to non-uniform stress distribution and subsequently reducing the mechanical properties. However, with the increase in CB content, the distribution of CB becomes more uniform within the polymer matrix, resulting in more uniform stress distribution and enhanced load-carrying capacity, leading to improved mechanical properties.

In the impact performance testing, the high-speed impact of the instrument causes stress concentration at the point of force application, leading to a sharp increase in local strain. This results in minimal deformation while allowing cracks to rapidly propagate. As shown in Fig. 6, the impact strength of the composite materials with a small amount of CB (1.5–3%) does not vary significantly. This is because both HDPE and PA6 possess good mechanical properties, and the addition of HDPE in the blend enhances the impact resistance of PA6 to some extent. Moreover, the impact resistance of the PA6/
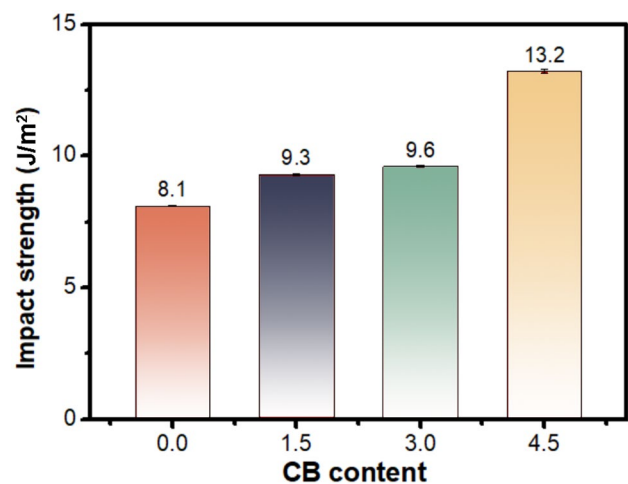


**Fig. 6** Comparison of impact strength of four groups of samples

HDPE/CB composite materials gradually increases with the increase of carbon black content, reaching a peak at 4.5% CB content. At 1.5% CB content, the impact resistance is slightly improved. This is due to the reinforcing effect of carbon black. When added to the PA6/PE composite, carbon black accumulates at the edges during injection molding, leading to stress concentration at its surface. Upon impact, carbon black absorbs some of the impact force before the PA6/HDPE composite fractures, thereby enhancing its toughness. However, when the content reaches 4.5%, the impact strength reaches its maximum value.

In order to characterize the transmittance of our material to EM waves in the microwave frequency

band [26–28], the complex permittivity and dielectric loss tangent of the 4 samples are very important basis for judgment (as shown in Figs. 7 and 8).

In general, the dielectric loss tangent value of less than 0.01 can become excellent wave-transmitting materials. The change of the transmittance of PHC-4.5 sample with thickness from 0 to 10 mm can be calculated according to the following formulas [29]:

$$R = \frac{1-n}{1+n} \quad (1)$$

$$n = \frac{\epsilon_r cos\theta}{\left(\epsilon_r - sin^2\theta\right)^{1/2}} \quad (2)$$
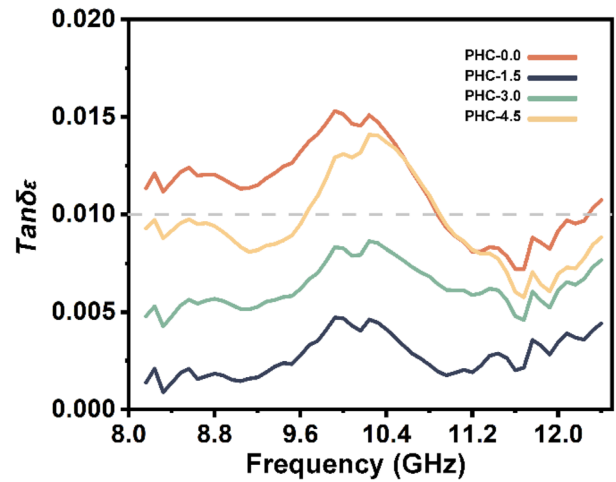


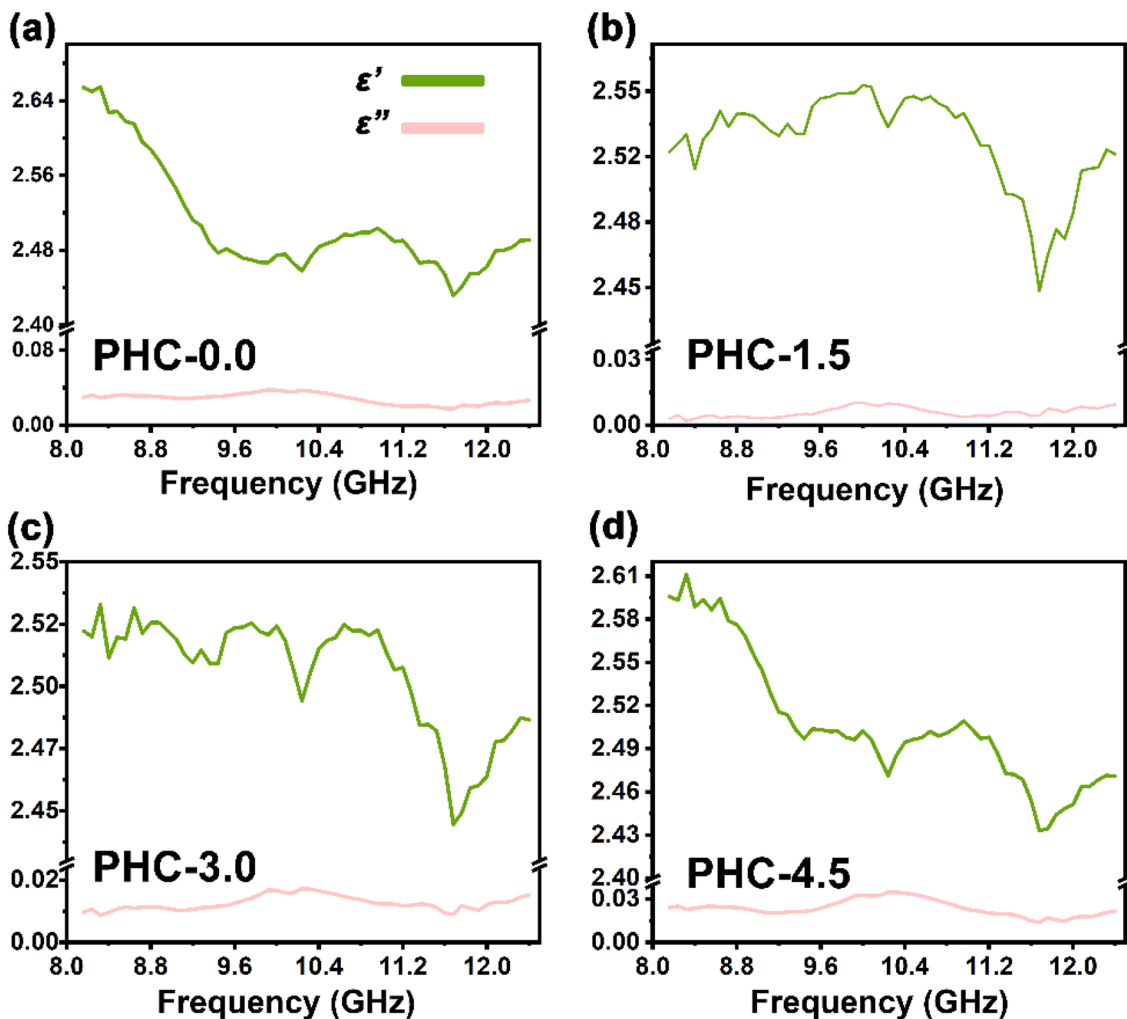**Fig. 8** Dielectric loss tangent of the four samples



**Fig. 7** Real ($\epsilon'$) and image ($\epsilon''$) part of relative complex permittivity of four samples

$$\left|T^2\right| = \frac{(1-R^2)}{(1-R^2)+4R^2 sin^2\phi} \quad (3)$$

$$\phi = \frac{2\pi d}{\lambda}\left(\epsilon_r - sin^2\theta\right)^{1/2} \quad (4)$$

where $R$ is the EM wave reflectance, $n$ is the refractive index, $\epsilon_r$ represents the relative permittivity, $\theta$ is the incident angle of impinging EM wave, $T$ is the EM wave transmittance, $\lambda$ is the wavelength and $\phi$ is phase. When EM wave is vertically incident, $\theta$ is equal to 0. Therefore, these formulas can be simplified to [30, 31]:

$$R = \frac{1-n}{1+n} \quad (5)$$

$$n = \epsilon_r^{1/2} \quad (6)$$

$$\left|T^2\right| = \frac{(1-R^2)}{(1-R^2)+4R^2 sin^2\phi} \quad (7)$$

$$\phi = \frac{2\pi d}{\lambda}n \quad (8)$$

By using this method, the trend of transmittance for the material in the X-band EM wave frequency range and thickness range of 0 to 1 mm can be calculated. As shown in Fig. 9, it effectively illustrates the relationship between the microwave transmittance of PHC-4.5 and its thickness and frequency [32–35]. The plane projection of the transmittance for PHC-4.5 is depicted in Fig. 9a. Regardless of the thickness in the range of 0 to 10 mm and the frequency in the range of 8.2 to 12.4 GHz, the transmittance of PHC-4.5 remains above 93.2%. This outstanding performance demonstrates the excellent microwave transmittance of PHC-4.5. From Fig. 9b, it can be observed that the transmittance of PHC-4.5 varies with changes in frequency and thickness. Due to its unique frequency-dependent characteristics, the transmittance does not always decrease with increasing thickness. Figure 9c shows the transmittance of PHC-4.5 at 1 mm thickness, and within the frequency range of 8.2 to 12.4 GHz, its microwave transmittance is consistently above 90% [36, 37]. This indicates that PHC-4.5 has broad potential applications as a wave-transparent material.

## 4 Conclusion

In summary, the effects of different CB contents on the mechanical properties, thermodynamics, and microwave transmittance of PA6/PE composite materials were investigated. At a CB content of 4.5%, the composite material exhibited significant improvements in overall tensile strength (53.3 MPa) and impact strength (13.2 J/m2) due to the uniform distribution of CB within the matrix, leading to more even stress distribution and partial absorption of impact forces. Moreover, the material demonstrated an extremely low overall dielectric loss tangent (below 0.01) at this CB content, attributed to the presence of island-like PE structures and dispersed CB particles that contribute to isotropic crystal symmetry, resembling an isotropic antenna with potential significance in EM wave transmission. Overall, these findings highlight the tremendous application potential of this PA6-based composite material in wideband transmission materials.
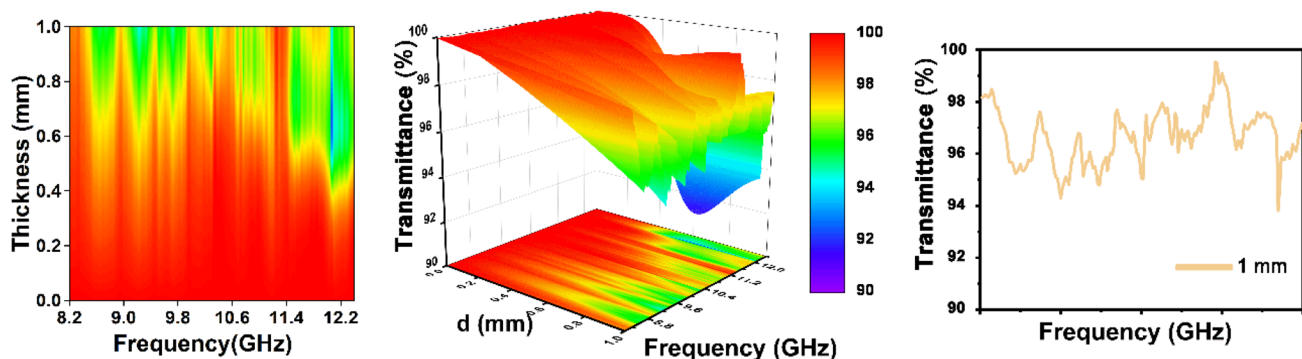


Fig. 9 **a** Plane projection map of microwave transmittance, **b** microwave transmittance of PHC-4.5 at 0–1 mm and **c** PHC-4.5 at 1 mm

## Author contributions

## Funding

## Data availability

Data will be made available on request.

## Declarations

**Competing interest**  The authors declare that they have no known competing financial interests or personal relationships that could have appeared to influence the work reported in this paper.

## References

1. S.M. Liu, J.Y. Huang, Z.J. Jiang, C. Zhang, J.Q. Zhao, J. Chen, J. Appl. Polym. Sci. **117**(6), 3370–3378 (2010)
2. K. Wang, J. Xie, T. Li, X. Wu, W. Huang, Q. Tian, C. Tu, W. Yan, J. Polym. Res. **27**, 1–8 (2020)
3. S. Pavlidou, C. Papaspyrides, Prog. Polym. Sci. **33**(12), 1119–1198 (2008)
4. K.S. Randhawa, A. Patel, Ind. Lubr. Tribol. **73**(9), 1146–1158 (2021)
5. L.N. Silva, E.G.R. dos Anjos, G.F.M. Morgado, J. Marini, E.H. Backes, L.S. Montagna, F.R. Passador, Polym. Bull. **77**, 3389–3409 (2020)
6. H. Yordanov, L. Minkova, Eur. Polym. J. **39**(5), 951–958 (2003)
7. N.S. Sanjani, A. Alipour, N. Nikfarjam, Polym. Plast. Technol. Eng. **52**(13), 1343–1352 (2013)
8. P.G. Malchev, G. de Vos, S.J. Picken, A.D. Gotsis, Compos. Sci. Technol. **70**(5), 734–742 (2010)
9. I. Kelnar, L. Kaprálková, J. Kratochvíl, J. Kotek, L. Kobera, J. Rotrekl, J. Hromádková, J. Appl. Polym. Sci. (2015). https://doi.org/10.1002/app.41868
10. J. Liang, Y. Xu, Z. Wei, P. Song, G. Chen, W. Zhang, J. Therm. Anal. Calorim. **115**, 209–218 (2014)
11. E. Fitzer, K.H. Kochling, H. Boehm, H. Marsh, Pure Appl. Chem. **67**(3), 473–506 (1995)
12. S. Ojha, S.K. Acharya, G. Raghavendra, J. Appl. Polym. Sci. **132**, 1 (2015)
13. N. Yan, J. Wu, Y. Zhan, H. Xia, Plast. Rubber Compos. **38**(7), 290–296 (2009)
14. F. Wang, R. Hong, W. Feng, D. Badami, K. Zeng, Mater. Lett. **125**, 48–50 (2014)
15. K. Yantaboot, T. Amornsakchai, Polym. Test. **61**, 223–228 (2017)
16. F. El-Tantawy, K. Kamada, H. Ohnabe, Mater. Lett. **56**(1–2), 112–126 (2002)
17. T. Bera, S. Acharya, P. Mishra, Int. J. Eng. Sci. Technol. **10**(4), 12–20 (2018)
18. Z. Elimat, S. Al-Hussami, A. Zihlif, J. Compos. Mater. **47**(28), 3525–3534 (2013)
19. K. Dai, Y. Qu, Y. Li, G. Zheng, C. Liu, J. Chen, C. Shen, Mater. Lett. **114**, 96–99 (2014)
20. F. Balta Calleja, R. Bayer, T. Ezquerra, J. Mater. Sci. **23**, 1411–1415 (1988)
21. L. Shen, F. Wang, H. Yang, Q. Meng, Polym. Test. **30**(4), 442–448 (2011)
22. Y. Hou, T. Zhao, Y. Shi, J. Fan, R. Zheng, Y. Zhang, Q. Gu, J. Appl. Polym. Sci. **135**(25), 46387 (2018)
23. D. Wu, Y. Wang, S. Deng, D. Lan, Z. Xiang, Q. He, Nano Res. **16**(2), 1859–1868 (2023)
24. L. Ren, Y. Wang, X. Zhang, Q. He, G. Wu, Int. J. Min. Metall. Mater. **30**(3), 504–514 (2023)
25. H. Du, J. Jiang, L. Ren, Q. He, Y. Wang, Colloids Surf, A **670**, 131564 (2023)
26. S. Zhang, B. Cheng, Z. Jia, Z. Zhao, X. Jin, Z. Zhao, G. Wu, Adv. Compos. Hybrid Mater. **5**(3), 1658–1698 (2022)
27. S. Zhang, Y. Pei, Z. Zhao, C. Guan, G. Wu, J. Colloid Interface Sci. **630**, 453–464 (2023)
28. S. Zhang, Z. Gao, Z. Sun, B. Cheng, Z. Zhao, Y. Jia, G. Wu, Appl. Surf. Sci. **611**, 155707 (2023)
29. D. Lan, M. Qin, R. Yang, H. Wu, Z. Jia, K. Kou, G. Wu, Y. Fan, Q. Fu, F. Zhang, J. Mater. Sci. Mater. Electron. **30**, 8771–8776 (2019)
30. D. Lan, H. Zhou, H. Wu, J. Colloid Interface Sci. **633**, 92–101 (2023)

31. Z. Gao, Z. Zhao, D. Lan, K. Kou, J. Zhang, H. Wu, J. Mater. Sci. Technol. **82**, 69–79 (2021)

32. N. Joseph, J. Varghese, M.T. Sebastian, Compos. B Eng. **123**, 271–278 (2017)

33. N. Joseph, J. Varghese, M.T. Sebastian, Polym. J. **49**(4), 391–399 (2017)

34. D. Lan, Y. Wang, Y. Wang, X. Zhu, H. Li, X. Guo, J. Ren, Z. Guo, G. Wu, J. Colloid Interface Sci. **651**, 494–503 (2023)

35. J. Varghese, N. Joseph, H. Jantunen, S. Behera, H. Kim, M. Sebastian, *Handbook of advanced ceramics and composites: defense, security, aerospace and energy applications* (Springer, Berlin, 2020), pp.165–213

36. J. Varghese, D.R. Nair, P. Mohanan, M.T. Sebastian, Phys. Chem. Chem. Phys. **17**(22), 14943–14950 (2015)

37. J. Zhou, D. Lan, F. Zhang, Y. Cheng, Z. Jia, G. Wu, P. Yin, Small (2023). https://doi.org/10.1002/smll.202304932